Atmos. Chem. Phys. Discuss., 14, 22547–22585, 2014
www.atmos-chem-phys-discuss.net/14/22547/2014/
doi:10.5194/acpd-14-22547-2014

Atmospheric Chemistry and Physics Discussions

Quantifying pyroconvective injection heights using observations of fire energy: sensitivity of space-borne observations of carbon monoxide

S. Gonzi[1], P. I. Palmer[1], R. Paugam[2], M. Wooster[2], and M. N. Deeter[3]

[1]School of GeoSciences, University of Edinburgh, Edinburgh, UK
[2]Department of Geography, King's College London, London, UK
[3]National Center for Atmospheric Research NCAR, Boulder, CO, USA

Received: 31 July 2014 – Accepted: 6 August 2014 – Published: 3 September 2014

Correspondence to: S. Gonzi (sgonzi@staffmail.ed.ac.uk)

Published by Copernicus Publications on behalf of the European Geosciences Union.

Abstract

We use observations of fire size and fire radiative power (FRP) from the NASA Moderate-Resolution Imaging Spectroradiometers (MODIS), together with a parameterized plume rise model, to estimate biomass burning injection heights during 2006. We use these injection heights in the GEOS-Chem atmospheric chemistry transport model to vertically distribute biomass burning emissions of carbon monoxide (CO) and to study the resulting atmospheric distribution. For 2006, we use over half a million FRP and fire size observations as input to the plume rise model. We find that convective heat fluxes and actual fire sizes typically lie in the range of 1–100 kW m^{-2} and 0.001–100 ha, respectively, although in rare circumstances the convective heat flux can exceed 500 kW m^{-2}. The resulting injection heights have a skewed probability distribution with approximately 80 % of injections remaining within the local boundary layer (BL), with occasional injection height exceeding 8 km. We do not find a strong correlation between the FRP-inferred surface convective heat flux and the resulting injection height, with environmental conditions often acting as a barrier to rapid vertical mixing even where the convective heat flux and actual fire size are large. We also do not find a robust relationship between the underlying burnt vegetation type and the injection height. We find that CO columns calculated using the MODIS-inferred injection height (MODIS-inj) are typically −9–+6 % different to the control calculation in which emissions are emitted into the BL, with differences typically largest over the point of emission. After applying MOPITT v5 scene-dependent averaging kernels we find that we are much less sensitive to our choice of injection height profile. The differences between the MOPITT and the model CO columns (max bias ≈ 50 %), due largely to uncertainties in emission inventories, are much larger than those introduced by the injection heights. We show that including a realistic diurnal variation in FRP (peaking in the afternoon) or accounting for subgrid-scale emission errors does not alter our main conclusions. Finally, we use a Bayesian maximum a posteriori approach constrained by MOPITT CO profiles to estimate the CO emissions but because of the inherent

ACPD
14, 22547–22585, 2014

bias between model and MOPITT we find little impact on the resulting emission estimates. Studying the role of pyroconvection in distributing gases and particles in the atmosphere using global MOPITT CO observations (or any current space-borne measurement of the atmosphere) is still associated with large errors, with the exception of a small subset of large fires and favourable environmental conditions, which will consequently lead to a bias in any analysis on a global scale.

1 Introduction

Fire plays an important role in the evolution of the Earth system (Bowman et al., 2009). We focus on the influence of fires on determining the atmospheric distribution of carbon monoxide (CO), a chemical tracer of incomplete combustion. In particular, we use space-borne measurements of fire radiative power (FRP) and estimates of the fires surface area over which this radiative output is produced, to describe the enhanced vertical mixing due to intense surface heating to (a) understand the resulting atmospheric variation in CO, and (b) quantify the impact on surface flux estimates inferred from atmospheric measurements of CO.

Satellite observations have played a central role in understanding the spatial extent and seasonality of fires across different ecosystems (e.g., Cahoon Jr. et al., 1992; Barbosa et al., 1999; Carmona-Moreno et al., 2005; Csiszar et al., 2006; van der Werf et al., 2006; Giglio, 2007; Boschetti et al., 2010; Ichoku et al., 2012). There is a substantial body of previous work on estimating biomass burning emissions of gases and particles using space-borne instruments with varying levels of success (e.g., Duncan et al., 2003; Martin et al., 2003; Freitas et al., 2005; Ito and Penner, 2004; Kasischke and Penner, 2004; Edwards et al., 2006; Hodzic et al., 2007; Jordan et al., 2008; Kopacz et al., 2009; Liousse et al., 2010; Gonzi et al., 2011b; Fleming et al., 2012; Ross et al., 2013), largely reflecting heterogeneous sampling due to cloud and aerosol contaminated observed scenes.

ACPD
14, 22547–22585, 2014

Recent studies have studied how injection heights can modify emitted gases and aerosols and downwind chemical composition (e.g., Palmer et al. (2013) and articles therein). Strictly speaking, pure pyroconvection is rare with most events triggered by storm systems that can result in unstable atmospheric conditions and enhance the vertical extent of the mixing due to the fire (e.g. Fromm et al., 2010; Dirksen et al., 2009). The importance of vertical mixing due to some extent by surface heating from fire has been shown by a number of previous studies that have used models with and without a description of pyroconvection to interpret aircraft and satellite data (e.g., Freitas et al., 2010; Fisher et al., 2010; Sessions et al., 2011; Zhang et al., 2011; Pfister et al., 2011). Within these studies, pyroconvection is typically treated in an ad hoc manner using a formulaic method of vertically redistributing surface emissions (e.g., Val Martin et al., 2012). FRP has been shown in small scale experiments to be related to rates of fuel combustion (Wooster et al., 2005) and to rates of key trace gas and aerosol emission (Freeborn et al., 2008). At the landscape scale previous work has shown that MODIS FRP measurements were related to the release rate of smoke aerosols (Ichoku and Kaufman, 2005), and recently MODIS FRP has been used to map daily landscape-scale fuel consumption rates (Kaiser et al., 2012) and via the application of biome-specific emissions factors, the rates of release of various chemical species present in the smoke.

In the following section, we describe the FRP and active fire area estimates derived from the MODIS measurements, and the CO data from the MOPITT satellite instrument. In Sect. 3 we describe the plume rise model and how we incorporate the resulting injection height inferred from the MODIS data into the GEOS-Chem atmospheric chemistry transport model. In Sect. 4, we report our results. We conclude in Sect. 5.

ACPD
14, 22547–22585, 2014

2 Data

2.1 MODIS fire observations

We use FRP values retrieved from MODIS on the Aqua and Terra satellites (Wooster et al., 2005; Ichoku et al., 2008). Both satellites are in a sun-synchronous, near-polar orbit. Terra and Aqua have an equatorial crossing time of 10:30 a.m. (10:30 p.m.) and 1:30 p.m. (1:30 a.m.) for their descending (ascending) nodes, respectively.

The FRP and Active Fire (AF) area for each fire are computed with the dual-band approach based on the bispectral algorithm of Dozier applied to the original MODIS calibrated Middle wave Infra Red (MIR) and Long Wave Infra Red (LWIR) radiance data (Dozier, 1981) stored in the active fire product (MOD14); a similar approach was already used by Val Martin et al. (2012). For each granule, the hot spot detected by the fire detection algorithm of MODIS is assigned to a particular fire based on the analysis of clusters of spatially contiguous fire pixels. This is the same approach as previously applied with data from the BIRD Hot spot Recognition Sensor (Wooster et al., 2003; Zhukov et al., 2005). It is designed to minimize some of the problems of the dual band method, for example those related to inter-channel spatial misregistration effects (Zhukov et al., 2005; Shephard and Edward, 2003). The average top of the atmosphere (TOA) radiances for each cluster are then corrected by the transmittance of the atmosphere in order to get the actual radiance emitted by the fire. The transmittance in each band is estimated from a precompiled lookup table based on the total amount of column water (from ECMWF reanalysis) and the view angle of the sensor (Govaerts et al., 2010). Both corrected MIR and LWIR radiance are then subject to analysis using the "dualband" approach (Dozier, 1981), using the specific method taken by Zhukov et al. (2005). Outputs for each cluster are the size and the temperature of the equivalent black body which has the same thermal emission signal as the observed fire in the MIR and LWIR. Finally, the size of the black body is used as an estimate of the active fire area and the FRP is computed using the MIR band (Wooster et al., 2005).

ACPD
14, 22547–22585, 2014

Previous work has shown this method of FRP estimation introduced an uncertainty of around ±10 % for fire temperature of 600–1600 K, with the advantage that the temperature of the fire does not need to be known (Wooster et al., 2005, 2003). The MODIS instrument is less sensitive to wildfires with temperature < 600 K, where gases emitted from smouldering is expected to be more substantial. We do not expect this high temperature bias will compromise our method of describing the associated vertical mixing which is typically limited to the BL; as described below, in the absence of an FRP value we distribute emissions in the first few vertical model layers.

Figure 1 shows the MODIS derived distribution of half a million colocated FRP and active burnt area data during 2006. The measurement density is highest over equatorial regions, with higher latitudes having less observations that reflect their seasonal cycle. We chose 2006 because FRP and fire size observations allows us to compare results with previous work (e.g., Gonzi et al., 2011a).

2.2 MOPITT column observations of CO

We use MOPITT v5 CO profile retrievals and the corresponding retrieval error covariances and scene dependent averaging kernels for 2006 (Deeter, 2011). CO concentrations are retrieved for ten pressure levels (surface, 900, 800, . . . 100 hPa) in the multispectral thermal-IR/near-IR (TIR/IR) regions based on log-normal statistics and an optimal estimation method. We do not consider the TIR- and NIR-only products here. The a priori CO information in the MOPITT retrieval algorithm is calculated with the global chemistry transport model MOZART (Horowitz et al., 2003) and meteorology in the retrieval algorithm is based on NCEP reanalysis data (Kalnay et al., 1996). The degree of freedom (DOF) for the multispectral TIR/IR retrievals is typically between 1.0–2.2; in comparison, NIR- and TIR-only products have DOFs peaking at 0.1–1.0 and 0.5–1.5, respectively (Deeter et al., 2012). Past analyses show that these MOPITT CO profiles have a bias against North American in-situ tall tower measurements (2000–2011) of typically −20 % to +20 % with a pronounced seasonal cycle (Deeter et al., 2013). To facililate ease of analysis we thin the MOPITT data and use a maximum of

ACPD
14, 22547–22585, 2014

three observations in a 1° × 1° grid cell for each day. We only use profile retrievals with a DOF > 1.3 and profiles for which the CO concentrations at 500 hPa are greater than 40 ppb (Gonzi et al., 2011a). This reduces the number of profiles considerably to approximately five million observations during 2006. We find that using a more relaxed DOF criteria so that more observations are collected per gridbox (not shown) does not signficantly affect our final analysis.

3 Models

3.1 Plume rise model

Pyroconvection is currently a sub-grid scale model process; resolving this process in a global model would involve prohibitive computational costs. Consequently, models tend to parameterize this process if they include it at all. We use an established 1-D plume rise model (Freitas et al., 2006, 2010), embedded within the GEOS-Chem atmospheric chemistry transport model described below, to describe the vertical mixing due to surface heating and consequently to redistribute surface emissions from the fire. The plume rise model estimates the injection height, defined as the level of neutral buoyancy, by solving equations for the vertical plume velocity, plume temperature, condensation and evaporation (latent heat), accounting for wind shear. We use a parameterization to conserve mass (Appendix A), which is an extension to the original code first published by (Freitas et al., 2006).

Initial surface boundary conditions in the plume rise model include MODIS derived convective heat flux (kW m^{-2}, defined below) and active burnt area (m^2), respectively, environmental temperature (K), relative humidity profile (%) and horizonal wind fields (m s^{-1}). We drive the plume model using meteorological data from version 5 of the NASA Goddard Earth Observing System Model (GEOS-5) (Rienecker et al., 2008), ensuring consistency with the GEOS-Chem meteorology. For each MODIS derived heat flux and area, an injection height value is calculated by the plume rise model. The

ACPD
14, 22547–22585, 2014

role of atmospheric water vapour vs. water released from fuel combustion is still subject to debate (e.g., Penner et al., 1986; Potter, 2005; Trentmann et al., 2006, 2009; Cunningham and Reeder, 2009). We assume a fuel moisture of 10 %, calculated from the colocated GEOS-5 relative humidity profile, which we add to the existing atmospheric levels. We further assume that the initial plume temperature equals the environmental temperature. The biggest source of moisture varation is from the atmosphere, which is updated with each time step during the fire as the plume temperature changes. Estimates of convective heat flux are also uncertain. Here, we use flux estimates inferred from FRP observations, assuming an underlying relationship between the two variables. Fire energy can broadly speaking be separated into three components: conduction, radiation and convection. The contribution from these sources to the total fire energy is uncertain, but it can be assumed that convection is as important as radiative energy (Anderson et al., 2010; Butler, 2010; Finney et al., 2012; Frankman et al., 2012). The maximum radiative heat yield that is typically measured by MODIS is about 20 % (Wooster et al., 2005) of the total heat whereas the maximum heat yield that can theoretically be liberated by a fire is between 20 % and 60 % (Ferguson et al., 2000). We assume that heat loss by conduction is relatively small compared to losses by the combined effect of radiation and convection. We assume an average heat loss of 15 % for radiation, 10 % for conduction, and 75 % due to convection (H_F, kW m^{-2}). The loss by convection is then given as $H_F = 5 \times \frac{\mathrm{FRP}}{A}$, where A (m^2) denotes the actual burnt fire size. We acknowledge here that this relation is probably the upper limit and will not hold true for every location and fire type around the globe, but it is a reasonable mean estimate based on current knowledge.

3.2 The GEOS-Chem atmospheric chemistry model

We use GEOS-Chem version 9-01-01 (www.geos-chem.org) as the forward model that relates surface emissions of CO to atmospheric concentrations of CO. The model is driven by meteorological analyses from the Goddard Earth Observing System v5 model maintained by the Global Modeling and Assimilation Office at NASA Goddard. We use

ACPD
14, 22547–22585, 2014

a horizontal resolution of 2°×2.5°, with 47 sigma levels that span the surface to 0.01 hPa of which 30 levels are within the troposphere. The 3-D meteorological data is updated every six hours, and heights of the BL and tropopause are updated every three hours.

We use monthly mean emission inventories for fossil fuel (Olivier and Berdowski, 2001; Streets et al., 2006), biofuel (Yevich and Logan, 2003), and biomass burning (van der Werf et al., 2010), and from the oxidation of volatile organic compounds (Duncan et al., 2007). Atmospheric oxidation by OH is the main atmospheric loss of CO, resulting in a lifetime of weeks to months depending on latitude and season. We use monthly 3-D fields of the OH sink precomputed from a full chemistry version of the model. Fixing the OH sink effectively allows us to linearly decompose the contributions of CO from source types and/or geographical regions. Figure 1 shows the eight geographical regions we study, reflecting the location of burning. For each region we track emissions from biomass burning and combined emissions from fossil fuel and biofuel combustion. We also track the combined contribution of CO from the oxidation of methane, isoprene, monoterpenes, methanol, and acetone. A more detailed description of this model can be found elsewhere (Duncan et al., 2007; Gonzi et al., 2011a). We sample the model at the time and location of MODIS and MOPITT measurements. Below, where we discuss model bias we define percentage bias as

$$\text{Bias} = 100 \times \frac{\text{CO}_\text{M} - \text{CO}_\text{X}}{\max(\text{CO}_\text{M}, \text{CO}_\text{X})}, \quad (1)$$

where CO_M denotes the model and CO_X denotes either the model control CO_C or the observed atmospheric measurement CO_O.

For the control run (and the default setting of GEOS-Chem), we release biomass burning emissions within the BL in which there are approximately 15 levels from the surface to 2.5 km. For the sensitivity runs using FRP to define the injection height we distribute surface emissions in the atmosphere using the plume rise model described above, driven by GEOS-5 meteorological analyses (Rienecker et al., 2008). The MODIS derived FRP data that falls into a specific model grid box during a three

ACPD
14, 22547–22585, 2014

hour window, determined by the GEOS-5 analyses, determines the surface convective heat flux boundary conditions. In the typical case of more than one FRP observation falling in a grid square during this time window, we create an injection height profile for each associated convective heat flux: equally distributing emitted mass from the surface to the injection height or from the local BL to the injection height whenever the injection height is larger than the BL. We then calculate an effective injection height by calculating a sum of individual profiles weighted by their respective fractional actual area burnt within that grid box. This fractional scaling ensures that the final effective profile conserves mass. If there are no FRP observations in a model grid box for a particular time but emissions are non-zero we distribute emissions within the local BL.

We also consider the sensitivity of our results to imposing a diurnal cycle on FRP, following analysis of similar data as a function of land cover type over Africa using the Spinning Enhanced Visible and Infrared Imager (SEVIRI) (Roberts et al., 2009). Figure 2 shows that the mean diurnal cycle peaks during early afternoon, consistent with previous analysis of data from the GOES WF_ABBA (Geostationary Operational Environment Satellite Wildfire Automated Biomass Burning Algorithm) active fire observations that show early afternoon peaks valid for the entire globe (Giglio, 2007; Mu et al., 2011). We use this mean diurnal profile to effectively relate observations taken at discrete times to the rest of the day, acknowledging this is a crude but reasonable assumption.

3.3 The maximum a posteriori (MAP) inverse model

We briefly describe our inverse model approach here that has been discussed at length elsewhere (Gonzi et al., 2011a). We sample the model along the MOPITT orbit by applying scene-dependent averaging kernels from MOPITT and follow an optimal estimation method in order to fit the model 3-D CO concentrations to the observations.

Figure 1 shows the eight geographical regions for which we estimate CO emissions: North America (NAM), EU (Europe), SIB (Siberia), INDO (Indonesia), AF (Africa), SAM (South America), AS (Asia) and CHEM (Rest of the world including chemistry). We

ACPD
14, 22547–22585, 2014

estimate lumped emissions from biomass burning, fossil fuel and biofuel emissions on a quarterly basis (JFM, AMJ, JAS, and OND). We assume a priori uncertainties of 50 % for incomplete combustion emissions and 25 % for the chemical oxidation source, following previous work (Gonzi and Palmer, 2010). For measurement errors, we include the local scene-dependent retrieval error from MOPITT to the final total error in log-space. We also include a 25 % uncertainty associated with the combined forward model and representation errors. The MAP algorithm described in a log-measurement space typically converges after a few iterations (Gonzi et al., 2011b).

4 Results

4.1 Convective heat fluxes, burned area, and injection heights for 2006

Figure 1 shows for 2006 the annual mean values for convection heat flux ($kW\,m^{-2}$) inferred from MODIS FRP measurements, and the corresponding actual burnt areas (hectares) used to determine the local pyroconvection injection height. The geographical variation of measurements available to calculate injection height reflects the frequency of fires and the magnitude of associated FRP derived heat flux, which is related to the fire regime of an area, and to the intensity of the energy emission from those fires. In general, the mean (not shown) and median values of the fire products are similar, suggesting there is little skewness in the distribution of FRP, although we acknowledge that the highest values are typically a factor of 5–10 higher than the mean value and that the median is in general the more robust statistic for this parameter. Figure 3 shows the corresponding global monthly box-and-whisker plots for convective heat flux and actual burnt area, respectively. The bulk of convective heat flux values are typically in the range 1–100 $kW\,m^{-2}$ and burnt areas typically lie in the range 0.1–10 ha. On occasion, active burnt area estimates can exceed 500 ha but these represent only a small percentage of the data.

ACPD
14, 22547–22585, 2014

Figure 1 shows the corresponding injection heights determined by the plume rise model. These data shows that the FRP-derived estimates of convective heat flux and actual fire size are insufficient by themselves to determine the injection height. This disagrees with field experiment data (Lavoué et al., 2000), but these were small-scale experiments with final injection heights that did not consider atmospheric stability constraints.

4.1.1 Sensitivity of injection heights to environmental parameters

Figure 4 shows two examples where values for MODIS FRP and/or actual fire size are similar but the analyzed meteorology for atmospheric temperature and specific humidity are different, resulting in different injection heights. Figure 4a show two instances where HF and A have similar values but the lower injection height (0.1 km vs. 3.3 km) is associated with a more stable atmosphere as determined by the negative gradient in potential temperature and higher specific humidity. This serves as an example where even modest changes in potential temperature can result in large changes to the model injection height. Figure 4b shows a contrasting example where there is clearly a positive gradient in potential temperature, indicative of a stable, stratified atmosphere, but the injection heights are much larger than the corresponding local BL heights. For these two cases values of HF and A are very large with the only difference being that the higher injection height (10 km vs. 6.9 km) having almost twice the HF. These two examples highlight the two limits that determine injection height: (1) small fires that rely on unstable environmental conditions to penetrate the free troposphere and (2) large fires (defined here as having high FRP and large active fire area) that can overcome locally stable environmental conditions to penetrate into the free troposphere. There are of course a continuum of possible combinations of variables between these two limits that determine the final injection height.

Figure 5 shows a statistical analysis of all the data analysed in 2006 to highlight the relationships between the injection height, convective heat flux and the actual fire area. We find an approximately linear relationship between the injection and fire area until

ACPD
14, 22547–22585, 2014

we reach areas > 80 hectares. We also find a similar relationship between the injection height and heat flux. This supports the idea that above a certain threshold of fire energy released the buoyancy induced by the fire can overcome locally stable meteorological conditions. Figure 5 also shows that the meteorological stability conditions play a progressively important role as the fire area and heat flux increases.

Previous work derived a plume height climatology based on a compilation of MODIS FRP and actual burnt area (Val Martin et al., 2012). These data were used to test the ability of a 1-D plume rise model in predicting the injection heights inferred from the Multi-angle Imaging SpectroRadiometer space-borne instrument (Diner et al., 2010) during the 2002, 2006 and 2007 North American burning seasons. They found that the plume rise model typically underpredicts the injection heights into the free troposphere due to the uncertain nature of input paramaters as FRP, fire size, and environmental meteorological conditions. They argue that a pre-compiled classification of injection heights as a function of parameters described in a look-up table may be an efficient approach to including injection heights in global models. While we agree that there is an urgent need for a predictive capability for plume rise, we believe that finding a robust relationship with injection height may well be as uncertain as using the plume rise model itself. We find that the biggest uncertainties is identifying the stability of the overlying atmosphere given the coarse meteorological information from global models.

Figure 6 shows that the normalized frequency distribution of injection heights over key burning regions are consistent, with differences only in the extent of the tails. This suggests that in almost all biomass burning regions smaller and less intense fires dominate with differences due mainly to the number of extreme fires, and how extreme they are. For example one might expect Canada to have a larger number of high intensity, large active fire area fires compared to Russia since we know Canada has a greater proportion of Crown fires than surface fires compared to Russia (e.g. Wooster and Zhang, 2004). For brevity we focus on a few regions. The median injection height for all regions is $\simeq 1.5$ km, with the highest injection heights of > 6 km over Indonesia, Africa, North America and Siberia. Once we subtract the local BL + 250 m layer (taking into

ACPD
14, 22547–22585, 2014

account uncertainty of the BL value) from this we find that typically 20 % of fires are injected above the BL consistent with bulk statistics reported in previous work (Val Martin et al., 2010). If we increase the free troposphere threshold to the local BL + 500 m we find that the fraction of fire reaching the free troposphere drops to 10–20 %; where Africa, Asia and North America is most affected suggesting these fires only just reach the free troposphere.

Val Martin et al. (2010) studied 584 MISR plumes over North America for the years 2002, 2006–2007 and their scaled-FRP/FRPx10 set-up found that 16–35 % (500–250 m BL uncertainty) reached the free troposphere compared to 24–48 % observed by MISR. We find that over North America during 2006, 14–22 % (500–250 m BL uncertainty) reach the free tropopshere. While the percentage of model plumes reaching the free troposphere over North America is similar to MISR they are not necessary the same group of plumes (Val Martin et al., 2010).

We use land cover classifications from AVHRR and MODIS observations (Hansen et al., 2000; Friedl et al., 2002) to investigate the relationship between the land cover (savannah, agriculture, peat, tropical and extratropical forest), FRP of fires and the resulting injection heights. We find that agricultural fires have a median FRP of 20 MW and are typically lower than over the other four biomes that have median values of 30 MW (not shown). The corresponding injection height mean statistics are similar for all vegetation types with the exception of agricultural for which heights < 5 km. Agricultural fires are small and typically low intensity, resulting in what would be expected to be low FRP for the fires when compared, for example, to many other types of fire. We also found no evidence to support that injection heights for extratropical forests were higher than from other biomes.

4.2 The sensitivity of atmospheric CO to pyroconvection

We use the GEOS-Chem atmospheric chemistry transport model (Sect. 3.2) to vertically distribute biomass burning emissions of CO according to the scene-dependent MODIS FRP-inferred injection height to understand the impact on atmospheric CO dis-

ACPD
14, 22547–22585, 2014

tributions. We then compare this model output to see whether it improves agreement with available data relative to the model that assumes an injection height that is limited to the BL.

To help evaluate our model during 2006, we use exclusively space-borne observations of CO from the v5 MOPITT CO profile retrievals (Deeter et al., 2013). The two major airborne campaigns MOZAIC (Marenco et al., 1998) and INTEX-B (Arellano Jr. et al., 2007) that measured CO during this period are not ideal for studying biomass burning. Previous work has showed that MOPITT data can be used to estimate emissions of CO from biomass burning (e.g., Pfister et al., 2005; Arellano Jr. et al., 2006; Chevallier et al., 2008; Kopacz et al., 2009; Gonzi et al., 2011a, b) but there still exists large uncertainties associated with the magnitude and timing of these emissions, reflecting model errors but also the coverage and uncertainties associated with MOPITT. As discussed in Sect. 3.2 we sample the model at the time and location of each MOPITT scene and convolve the resulting profile in log space with scene-specific averaging kernels.

Figure 7 shows that the model using the injection height estimate inferred from MODIS as a daily mean value has the largest differences (−5–+2 %), relative to the control, over and downwind of central and southern Africa. Including our diurnal variation of FRP (Fig. 2) increases the magnitude and spatial extent of the differences over and downwind of Africa and also introduces differences over Siberia and to a lesser extent over Southeast Asia and Australia. A cross section plot along the latitudes vs. altitude (Fig. 7) shows that the largest averaged monthly negative bias occurs in the BL at $\approx -12^{\circ}$ latitude, corresponding to the largest negative bias in the total columns. If we then convolve the model profiles with scene-dependent MOPITT averaging kernels these differences (not shown) are substantial reduced to $< \pm 2$ %. We find that the differences (±50 %) between model values as would be observed by MOPITT space with MOPITT data are an order of magnitude larger (third panel Fig. 7) than those introduced by using different formulations of injection height. In general, we find that the model bias against MOPITT, largely due to errors in prior emission inventories, is an

ACPD
14, 22547–22585, 2014

order of magnitude larger than the model response convolved with MOPITT averaging kernels to different prescriptions of injection height. Previous work used the GEOS-Chem model to infer CO emissions from MOPITT v5 CO profiles between June and August 2006 (Jiang et al., 2012). They found that posterior emission estimates were sensitive to the pressure level used: GEOS-Chem over(under)-estimates CO at lower (middle and upper) levels.

Figure 8 shows an example of model and MOPITT CO profiles over Siberian forest fires. The model CO mixing ratio with and without MODIS-inferred injection height using our diurnal distribution is 30–80 ppb in the lower troposphere. After we relate model CO concentrations to CO columns which are observed by MOPITT using the relevant averaging kernel (Fig. 8) the difference between the two models reduces to < 10 ppb. We find the resulting model profile overestimates (underestimates) CO at the surface (in the free troposphere), relative to MOPITT. The corresponding column amounts are 3.3×10^{18} molec cm^{-2} for MOPITT and 2.4×10^{18} molec cm^{-2} (2.3×10^{18} molec cm^{-2}) for the model with (without) scene-dependent injection height. For this example, it is clear that the model minus MOPITT bias of 27 % is much larger than the 5 % difference between the two model calculations. We find similar instances over the other burning loci around the world. We show this example profile because it corresponds to the time and location of the largest bias (≈ 5 %) between model w/wo injection height over the region SIB (Fig. 7). MOPITT profiles have generally finer vertical resolution.

For the above calculations we have assumed that material is distributed uniformally from the surface to the prescribed injection height. We consider two alternative formulations. First, we take into account that the majority of surface fires will typically be $< 2^\circ \times 2.5^\circ$ ($\approx 62\,500$ km^2), and acknowledge that only the most intense of these will play a substantial role in determining atmospheric composition. We select the fires within the top 20th percentile of global injection heights (> 2.2 km) and artifically (and crudely) increase the associated emissions by a factor of four. We denote this simulation as InJS1. Second, we take into account that the injection height is only a crude measure of the atmospheric flow, and that detrainment of the vertical flow generated

ACPD
14, 22547–22585, 2014

by eddies in the mixing processes will deposit emissions at heights below the highest value. To address this we incorporate a normalized parabolic injection height profile with a half-width maximum of 1 km such that the profile integrates to unity (InJS2). For both sensitivity runs we produce a corresponding control run that can be used to assess the importance of the parameter being perturbed. We find that the maximum total column bias in Fig. 7 is about a factor of two larger for InjS1 than for InjS2 (not shown), although the spatial distribution of the bias is the same, as expected, but is still small compared to the model minus MOPITT differences.

We have reported that MOPITT averaging kernels are often broader than the vertical sensitivity necessary to distinguish between different prescribed vertical injection heights due to surface heating. This is reflected in more detailed analyses involve MAP algorithms for which we find only small adjustments to posterior emissions compared to differences due to emissions that have been published previously (e.g., Gonzi et al., 2011a). We therefore do not discuss this any further.

5 Concluding remarks

We presented the first global, annual study of space-borne observations of fire radiative power and fire size to study the resulting injection heights. We used MODIS FRP and fire size observations for 2006 to improve understanding their relationship and the resulting injection height by embedding a 1-D plume-rise model into a global 3-D chemistry transport model. We did not find a robust relationship between FRP, fire size and injection height, and suggest that any effort to find one may be as uncertain as using these data as for scene-specific initial conditions for a 1-D plume-rise model.

We demonstrated using the plume rise model that different prescriptions of injection height do have an impact on atmospheric CO concentrations over intense fires. In general, model bias against MOPITT can be as large as 50 %, which dwarves any realistic perturbation from the redistribution of CO mass within a vertical column after being convolved with scene-dependent MOPITT averaging kernels. We have shown exam-

ACPD
14, 22547–22585, 2014

ples over large fires where MOPITT can differentiate between different prescriptions of vertical transport of CO emissions. As a consequence we cannot quantify the impact of injection heights on the inference of CO emissions from MOPITT CO profile data via an inverse model. The major implication from this result is that outside of detailed case studies, use of MOPITT to quantify biomass burning emissions is biased towards the very largest fires that can perturb substantial sections of the observed atmospheric column.

Space borne observations of FRP, fire area and other land-surface properties together with atmospheric concentration measurement remain our best constraints for biomass burning emissions and associated vertical transport. More effective use of the land-surface properties used in this study may require assimilation with a model that explicitly includes the observed parameters.

A new space-borne mission that retrieves biomass burning trace gases and associated land-surface properties would be required to address some of the gaps in current understanding. Previous analysis of the atmospheric signature from biomass burning using space-borne data has focused on CO using thermal IR sensors such as MOPITT with greatest sensitivity in the free troposphere, or short-lived trace gases such as formaldehyde measured by UV/Vis sensors that require a detailed knowledge of atmospheric chemistry (e.g., Gonzi et al., 2011b). The ideal mission would have a vertical resolution < 1 km in the lower and free troposphere and a ground-pixel size of 1 km or less. To achieve this a combined nadir/limb viewing instrument that measures thermal and short-wave IR wavelength may be required but integrating these data bring their own challenges (e.g., Gonzi and Palmer, 2010).

Appendix

The plume rise model variables are solved on a vertical grid comprising 200 levels in steps of 100 m. We extended the original model by introducing a mass conservation

ACPD
14, 22547–22585, 2014

variable ζ (Paugam et al., 2010).

$$\frac{\partial w}{\partial t} + w\frac{\partial w}{\partial z} = \frac{1}{1+\gamma} gB - \epsilon w^2 \tag{A1a}$$

$$\frac{\partial T}{\partial t} + w\frac{\partial T}{\partial z} = -w\frac{g}{c_p} - \epsilon w(T - \bar{T}) + \frac{\partial T}{\partial t}_{\text{micro}} \tag{A1b}$$

$$\frac{\partial \zeta}{\partial t} = \frac{\partial w\zeta}{\partial z} + w\zeta(\epsilon - \delta) \tag{A1c}$$

$$\frac{\partial \phi}{\partial t} + w\frac{\partial \phi}{\partial z} = -\epsilon w(\phi - \phi_e) \tag{A1d}$$

$$\zeta = \rho R^2 \tag{A1e}$$

$$\epsilon = \max\left(0, C_\epsilon \frac{B}{w^2}\right) + C_\epsilon \frac{1}{w}\frac{\mathrm{d}u}{\mathrm{d}z} \tag{A1f}$$

$$\delta = \max\left(0, C_\delta \frac{B}{w^2}\right) + C_\delta C_\epsilon \frac{1}{w}\frac{\mathrm{d}u}{\mathrm{d}z}, \tag{A1g}$$

where w denotes vertical plume velocity ($\mathrm{m\,s^{-1}}$), T (K) is the plume temperature, T_e (K) is the environmental temperature, B (kg) is the buoyancy (gB), g ($\mathrm{m\,s^{-2}}$) gravitational constant, γ (unitless) scaling factor, c_p ($\mathrm{J\,kg^{-1}\,K^{-1}}$) specific heat for constant pressure, ζ mass ($\mathrm{kg\,m^{-1}}$), ϵ ($1\,\mathrm{s^{-1}}$) and δ ($1\,\mathrm{s^{-1}}$) denote entrainment and detrainment, respectively, where C_ϵ (–) and C_δ (–) are empirical, unitless scaling factors (Pergaud et al., 2009). The subscript *micro* takes into account: evaporation, condensation, rain, ice with respect to the saturation water mass mixing ratio.

The initial boundary conditions rely on GEOS-5 temperatures, relative humidity (available water), and wind fields. The actual area size and convective heat flux, respectively is based on MODIS derived observations (see main text). As we mentioned in the main text we calculate the available water ($\mathrm{g\,m^{-2}}$) from the fuel by a simple formula and add it to the environmental available water in the first vertical model grid

ACPD
14, 22547–22585, 2014

box:

$$\text{water} = \frac{H_f \times \frac{dt}{H} \times (0.5 + f_{moist})}{0.55} \times 1000, \quad \text{(A2)}$$

where H_f is the convective heat flux ($W\,m^{-2}$), H is the fuel its heat storage capacity ($J\,kg^{-1}$), dt is the time step in (s), and f_{moist} is the moisture content of the fuel (–). We assume f_{moist} has a ratio of 10 %. The factor 0.5 in the equation assumes 0.5 kg is being emitted as water per 1 kg fuel burnt. For H we choose a value of 19 $MJ\,kg^{-1}$ representing typical fuel vegetation characteristics.

Acknowledgements. We thank Saulo Freitas (INPE/CPTEC) for useful discussions regarding the plume rise model code. This work was supported by the UK Natural Environment Research Council grant NE/E01819X/1. PIP gratefully acknowledges his Royal Society Wolfson Research Merit Award.

References

Anderson, W. R., Catchpole, E. A., and Butler, B. W.: Convective heat transfer in fire spread through fine fuel beds, Int. J. Wildland Fire, 9, 284–298, 2010. 22554

Arellano Jr., A. F., Kasibhatla, P. S., Giglio, L., van der Werf, G. R., Randerson, J. T., and Collatz, G. J.: Time-dependent inversion estimates of global biomass-burning CO emissions using Measurement of Pollution in the Troposphere (MOPITT) measurements, J. Geophys. Res., 111, D09303, doi:10.1029/2005JD006613, 2006. 22561

Arellano Jr., A. F., Raeder, K., Anderson, J. L., Hess, P. G., Emmons, L. K., Edwards, D. P., Pfister, G. G., Campos, T. L., and Sachse, G. W.: Evaluating model performance of an ensemble-based chemical data assimilation system during INTEX-B field mission, Atmos. Chem. Phys., 7, 5695–5710, doi:10.5194/acp-7-5695-2007, 2007. 22561

Barbosa, P. M., Stroppiana, D., and Gregoire, J.-M.: An assessment of vegetation fire in Africa (1981–1991): burned areas, burned biomass, and atmospheric emissions, Global Biogeochem. Cy., 13, 933–950, 1999. 22549

ACPD
14, 22547–22585, 2014

Boschetti, L., Roy, D. P., Justice, C. O., and Giglio, L.: An assessment of vegetation fire in Africa (1981–1991): burned areas, burned biomass, and atmospheric emissions, Int. J. Wildland Fire, 19, 705–709, 2010. 22549

Bowman, D. M. J. S., Balch, J. K, Artaxo, P., Bond, W. J., Carlson, J. M., Cochrane, M. A., D'Antonio, C. M., DeFries, R. S., Doyle, J. C., Harrison, S. P., Johnston, F. H., Keeley, J. E., Krawchuk, M. A., Kull, C. A., Marstona, J. B., Moritz, M. A., Prentice, I. C., Roos, C. I., Scott, A. C., Swetnam, T. W., van der Werf, G. R., and Pyne, S. J.: Fire in the Earth System, Science, 324, 481–484, 2009. 22549

Butler, B. W.: Characterization of convective heating in full scale wildland fires, in: International Conference on Forest Fire Research, edited by: Viegas, D. X., 15–18 November 2010, Coimbra, Portugal, 2010. 22554

Cahoon Jr., D., Stocks, B., Levine III, J., W. C., and O'Neill, K.: Seasonal distribution of African savanna fires, Nature, 359, 812–815, 1992. 22549

Carmona-Moreno, C., Belward, A., Malingreau, J., Hartley, A., Garcia-Algere, M., Antonovskiy, M., Buchshtaber, V., and Pivovarov, V.: Characterizing interannual variations in global fire calendar using data from Earth observing satellites, Glob. Change Biol., 11, 1537–1555, 2005. 22549

Chevallier, F., Fortems, A., Bousquet, P., Pison, I., Szopa, S., Devaux, M., and Hauglustaine, D. A.: African CO emissions between years 2000 and 2006 as estimated from MOPITT observations, Biogeosciences, 6, 103–111, doi:10.5194/bg-6-103-2009, 2009. 22561

Csiszar, I. A., Morisette, J. T., and Giglio, L.: Validation of active fire detection from moderate-resolution satellite sensors: the MODIS example in northern Eurasia, IEEE T. Geosci. Rem. Sens., 44, 1757–1764, 2006. 22549

Cunningham, P. and Reeder, M. J.: Severe convective storms initiated by intense wildfires: numerical simulations of pyro-convection and pyro-tornadogenesis, Geophys. Res. Lett., 36, L12812, doi:10.1029/2009GL039262, 2009. 22554

Deeter, M. N.: MOPITT Measurements of Pollution in the Troposphere, Version 5 Product User's Guide, Tech. rep., https://www2.acd.ucar.edu/sites/default/files/mopitt/v5_users_guide_beta.pdf, last access: 31 August 2011. 22552

Deeter, M. N., Worden, H. M., Edwards, D. P., Gille, J. C., and Andrews, A. E.: Evaluation of MOPITT retrievals of lower-tropospheric carbon monoxide over the United States, J. Geophys. Res., 117, D13306, doi:10.1029/2012JD017553, 2012. 22552

ACPD
14, 22547–22585, 2014

Deeter, M. N., Martinez-Alonso, S., Edwards, D. P., Emmons, L. K., Gille, J. C., Worden, H. M., Pittman, J. V., Daube, B. C., and Wofsy, S. C.: Validation of MOPITT version 5 thermal-infrared, near-infrared, and multispectral carbon monoxide profile retrievals for 2000–2011, J. Geophys. Res., 118, 6710–6725, doi:10.1002/jgrd.50272, 2013. 22552, 22561

Diner, D., Ackerman, T., Braverman, A., Bruegge, C., Chopping, M., Clothiaux, E., Davies, R., Girolamo, L. D., Kahn, R., Knyazikhin, Y., Liu, Y., Marchand, R., Martonchik, J., Muller, J., Nolin, A., Pinty, B., Verstraete, M., Wu, D., Garay, M., Kalashnikova, O., Davis, A., Davis, E., and Chipman, R.: Ten years of MISR observations from Terra: looking back, ahead, and in between, Proc. IEEE Int. Geosci. Remote Sens. Symp., pp. 1297–1299, 2010. 22559

Dirksen, R. J., Boersma, K. F., de Laat, P., Stammes, J., van der Werf, G., Martin, M. V., and Kelder, H. M.: An aerosol boomerang: rapid around-the-world transport of smoke from the December 2006 Australian forest fires observed from space, J. Geophys. Res., 114, D21201, doi:10.1029/2009JD012360, 2009. 22550

Dozier, J.: A method for satellite identification of surface temperature fields of subpixel resolution, Remote Sens. Environ., 11, 221–229, 1981. 22551

Duncan, B. N., Martin, R. V., Staudt, A. C., Yevich, R., and Logan, J. A.: Interannual and seasonal variability of biomass burning emissions constrained by satellite observations, J. Geophys. Res., 108, 4040, doi:10.1029/2002JD002378, 2003. 22549

Duncan, B. N., Logan, J. A., Bey, I., Megretskaia, I. A., Yantosca, R. M., Novelli, P. C., Jones, N. B., and Rinsland, C. P.: Global budget of CO, 1988–1997: source estimates and validation with a global model, J. Geophys. Res., 112, D22301, doi:10.1029/2007JD008459, 2007. 22555

Edwards, D. P., Emmons, L. K., Gille, J. C., Chu, A., Attié, J.-L., Giglio, L., Wood, S. W., Haywood, J., Deeter, M. N., Massie, S. T., Ziskin, D. C., and Drummond, J. R.: Satellite-observed pollution from Southern Hemisphere biomass burning, J. Geophys. Res., 111, D14312, doi:10.1029/2005JD006655, 2006. 22549

Ferguson, S., Sandberg, D., and Ottmar, R.: Modelling the effect of land use changes on global biomass emissions, in: Biomass Burning and Its Inter-relationship With the Climate System, Springer, New York, 33–50, 2000. 22554

Finney, M. A., Cohen, J. D., McAllister, S. S., and Jolly, W. M.: On the need for a theory of wildland fire spread, Int. J. Wildland Fire, doi:10.1071/WF11117, 2012. 22554

Fisher, J. A., Jacob, D. J., Purdy, M. T., Kopacz, M., Le Sager, P., Carouge, C., Holmes, C. D., Yantosca, R. M., Batchelor, R. L., Strong, K., Diskin, G. S., Fuelberg, H. E., Holloway, J. S.,

ACPD
14, 22547–22585, 2014

Hyer, E. J., McMillan, W. W., Warner, J., Streets, D. G., Zhang, Q., Wang, Y., and Wu, S.: Source attribution and interannual variability of Arctic pollution in spring constrained by aircraft (ARCTAS, ARCPAC) and satellite (AIRS) observations of carbon monoxide, Atmos. Chem. Phys., 10, 977–996, doi:10.5194/acp-10-977-2010, 2010. 22550

Fleming, Z. L., Monks, P. S., and Manning, A. J.: Review: untangling the influence of air-mass history in interpreting observed atmospheric composition, Atmos. Res., 104–105, 1–39, doi:10.1016/j.atmosres.2011.09.009, 2012. 22549

Frankman, D., Webb, B. W., Butler, B. W., Jimenez, D., Forthofer, J. M., Sopko, P., Shannon, K. S., Hiers, J. K., and Ottmar, R. D.: Measurements of convective and radiative heating in wildland fires, Int. J. Wildland Fire, 22, 157–165, doi:10.1071/WF11097, 2012. 22554

Freeborn, P. H., Wooster, M. J., Hao, W. M., Ryan, C. A., Nordgren, B. L., Baker, S. P., and Ichoku, C.: Relationships between energy release, fuel mass loss, and trace gas and aerosol emissions during laboratory biomass fires, J. Geophys. Res., 113, D01301, doi:10.1029/2007JD008679, 2008. 22550

Freitas, S., Longo, K. M., Dias, M. A. F. S., Dias, P. L. S., Chatfield, R., Prins, E., Artaxo, P., Grell, G. A., and Recuero, F. S.: Monitoring the transport of biomass burning emissions in South America, Environ. Fluid. Mech., 5, 135–167, 2005. 22549

Freitas, S. R., Longo, K. M., and Andreae, M. O.: Impact of including the plume rise of vegetation fires in numerical simulations of associated atmospheric pollutants, Geophys. Res. Lett., 33, L17808, doi:10.1029/2006GL026608, 2006. 22553

Freitas, S. R., Longo, K. M., Trentmann, J., and Latham, D.: Technical Note: Sensitivity of 1-D smoke plume rise models to the inclusion of environmental wind drag, Atmos. Chem. Phys., 10, 585–594, doi:10.5194/acp-10-585-2010, 2010. 22550, 22553

Friedl, M., McIver, D., Hodges, J., Zhang, X., Muchoney, D., Strahler, A., Woodcock, C., Gopal, S., Schneider, A., Cooper, A., Baccini, A., Gao, F., and Schaaf, C.: Global land cover mapping from MODIS: algorithms and early results, Remote Sens. Environ., 83, 287–302, 2002. 22560

Fromm, M., Lindsey, D. T., Yue, R. S. G., Sica, T. T. R., Doucet, P., and Godin-Beekmann, S.: The Untold Story of Pyrocumulonimbus, B. Am. Meteorol. Soc., 91, 1193–1209, doi:10.1175/2010BAMS3004.1, 2010. 22550

Giglio, L.: Characterization of the tropical diurnal cycle using VIRS and MODIS observations, Remote Sens. Environ., 108, 407–421, 2007. 22549, 22556

ACPD
14, 22547–22585, 2014

Gonzi, S. and Palmer, P. I.: Vertical transport of surface fire emissions observed from space, J. Geophys. Res., 115, D02306, doi:10.1029/2009JD012053, 2010. 22557, 22564

Gonzi, S., Feng, L., and Palmer, P. I.: Seasonal Cycle of Emissions of CO inferred from MOPITT profiles of CO: sensitivity to pyroconvection and profile retrieval assumptions, Geophys. Res. Lett., 38, L08813, doi:10.1029/2011GL046789, 2011a. 22552, 22553, 22555, 22556, 22561, 22563

Gonzi, S., Palmer, P. I., Barkley, M. P., Smedt, I. D., and Roosendael, M. V.: Biomass burning emission estimates inferred from satellite column measurements of HCHO: sensitivity to co-emitted aerosol and injection height, Geophys. Res. Lett., 38, L14807, doi:10.1029/2011GL047890, 2011b. 22549, 22557, 22561, 22564

Govaerts, Y., Lattanzio, M. W. P. F. A., and Roberts, G.: Algorithm theoretical basis document for MSG SEVIRI Fire Radiative Power (FRP) characterization, Technical Report Series on Global Modeling and Data Assimilation, EUMETSAT (LSA SAF), 2010. 22551

Hansen, M., DeFries, R., Townshend, J., and Sohlberg, R.: Global land cover classification at 1 km resolution using a decision tree classifier, Int. J. Remote Sens., 21, 1331–1365, 2000. 22560

Hodzic, A., Madronich, S., Bohn, B., Massie, S., Menut, L., and Wiedinmyer, C.: Wildfire particulate matter in Europe during summer 2003: meso-scale modeling of smoke emissions, transport and radiative effects, Atmos. Chem. Phys., 7, 4043–4064, doi:10.5194/acp-7-4043-2007, 2007. 22549

Horowitz, L. W., Walters, S., Mauzerall, D. L., Emmons, L. K., Rasch, P. J., Granier, C., Tie, X., Lamarque, J.-F., Schultz, M. G., Tyndall, G. S., Orlando, J. J., and Brasseur, G. P.: A global simulation of tropospheric ozone and related tracers: Description and evaluation of MOZART, J. Geophys. Res., 108, doi:10.1029/2002JD002853, 2003. 22552

Ichoku, C. and Kaufman, Y.: A method to derive smoke emission rates from MODIS fire radiative energy measurements, IEEE T. Geosci. Rem. Sens., 43, 2636–2649, 2005. 22550

Ichoku, C., Giglio, L., Wooster, M. J., and Remer, L. A.: Global characterization of biomass-burning patterns using satellite measurements of fire radiative energy, Remote Sens. Environ., 112, 2950–2962, doi:10.1016/j.atmosres.2012.03.007, 2008. 22551

Ichoku, C., Kahn, R., and Chin, M.: Characterisation of GOME-2 formaldehyde retrieval sensitivity, 111, 1–28, doi:10.1016/j.atmosres.2012.03.007, 2012. 22549

ACPD
14, 22547–22585, 2014

Ito, A. and Penner, J. E.: Global estimates of biomass burning emissions based on satellite imagery for the year 2000, J. Geophys. Res., 109, D14S05, doi:10.1029/2003JD004423, 2004. 22549

Jiang, Z., Jones, D. B. A., Worden, H. M., Deeter, M. N., Henze, D. K., Worden, J., Bowman, K. W., Brenninkmeijer, C. A. M., and Schuck, T.: Impact of model errors in convective transport on CO source estimates inferred from MOPITT CO retrievals, J. Geophys. Res., 118, 2073–2083, doi:10.1002/jgrd.50216, 2012. 22562

Jordan, N., Ichoku, C., and Hoff, R.: Estimating smoke emissions over the U.S. southern Great Plains using MODIS fire radiative power and aerosol observations, Atmos. Environ., 42, 2007–2022, 2008. 22549

Kaiser, J. W., Heil, A., Andreae, M. O., Benedetti, A., Chubarova, N., Jones, L., Morcrette, J.-J., Razinger, M., Schultz, M. G., Suttie, M., and van der Werf, G. R.: Biomass burning emissions estimated with a global fire assimilation system based on observed fire radiative power, Biogeosciences, 9, 527–554, doi:10.5194/bg-9-527-2012, 2012. 22550

Kalnay, E., Kanamitsu, M., Kistler, R., Collins, W., Deaven, D., Gandin, L., Iredell, M., Saha, S., White, G., Woollen, J., Zhu, Y., Leetmaa, A., Reynolds, B., Chelliah, M., Ebisuzaki, W., Higgins, W., Janowiak, J., Mo, K. C., Ropelewski, C., Wang, J., Jenne, R., and Joseph, D.: The NCEP/NCAR 40-years Reanalysis Project, B. Am. Meteorol. Soc., 77, 437–471, 1996. 22552

Kasischke, E. and Penner, J. E.: Improving global estimates of atmospheric emissions from biomass burning, J. Geophys. Res., 109, D14S01, doi:10.1029/2004JD004972, 2004. 22549

Kopacz, M., Jacob, D., Henze, D., Heald, C., Streets, D., and Zhang, Q.: Comparison of analytical and adjoint Bayesian inversion methods for constraining Asian sources of CO using satellite (MOPITT) measurements of CO columns, J. Geophys. Res., 114, 1–10, 2009. 22549, 22561

Lavoué, D. C., Liousse, C., Cachier, H., Stocks, B., and Goldhammer, J.: Modelling of carbonaceous particles emitted by boreal and temperature wildfires at northern latitudes, J. Geophys. Res., 105, 26871–26890, 2000. 22558

Liousse, C., Guillaume, B., Grégoire, J. M., Mallet, M., Galy, C., Pont, V., Akpo, A., Bedou, M., Castéra, P., Dungall, L., Gardrat, E., Granier, C., Konaré, A., Malavelle, F., Mariscal, A., Mieville, A., Rosset, R., Serça, D., Solmon, F., Tummon, F., Assamoi, E., Yoboué, V., and Van Velthoven, P.: Updated African biomass burning emission inventories in the framework

ACPD
14, 22547–22585, 2014

of the AMMA-IDAF program, with an evaluation of combustion aerosols, Atmos. Chem. Phys., 10, 9631–9646, doi:10.5194/acp-10-9631-2010, 2010. 22549

Marenco, A., Thouret, V., Nedelec, P., Smit, H., Helten, M., Kley, D., Karcher, F., Simon, P., Law, K., Pyle, J., Poschmann, G., Wrede, R. V., Hume, C., and Cook, T.: Measurements of ozone and water vapour by Airbus in-service aircraft: the MOZAIC airborne program, J. Geophys. Res., 103, 25631–25642, 1998. 22561

Martin, R., Jacob, D., Chance, K., Kurosu, T., Palmer, P., and Evans, M.: Global inventory of nitrogen oxide emissions constrained by space-based observations of NO_2 columns, J. Geophys. Res., 108, 4537, doi:10.1029/2003JD003453, 2003. 22549

Mu, M., Randerson, J. T., van der Werf, G. R., Giglio, L., Kasibhatla, P., Morton, D., Collatz, G. J., DeFries, R. S., Hyer, E. J., Prins, E. M., Griffith, D. W. T., Wunch, D., Toon, G. C., Sherlock, V., and Wennberg, P.: Daily and 3-hourly variability in global fire emissions and consequences for atmospheric model predictions of carbon monodixde, J. Geophys. Res., 116, D24303, doi:10.1029/2011JD016245, 2011. 22556

Olivier, J. and Berdowski, J.: Global emissions sources and sinks, In: Berdowski, J., Guicherit, R. and B.J. Heij (eds.) The Climate System, 33–78, A.A. Balkema Publishers/Swets & Zeitlinger Publishers, Lisse, The Netherlands, ISBN 90 5809 255, 2001. 22555

Palmer, P. I., Parrington, M., Lee, J. D., Lewis, A. C., Rickard, A. R., Bernath, P. F., Duck, T. J., Waugh, D. L., Tarasick, D. W., Andrews, S., Aruffo, E., Bailey, L. J., Barrett, E., Bauguitte, S. J.-B., Curry, K. R., Di Carlo, P., Chisholm, L., Dan, L., Forster, G., Franklin, J. E., Gibson, M. D., Griffin, D., Helmig, D., Hopkins, J. R., Hopper, J. T., Jenkin, M. E., Kindred, D., Kliever, J., Le Breton, M., Matthiesen, S., Maurice, M., Moller, S., Moore, D. P., Oram, D. E., O'Shea, S. J., Owen, R. C., Pagniello, C. M. L. S., Pawson, S., Percival, C. J., Pierce, J. R., Punjabi, S., Purvis, R. M., Remedios, J. J., Rotermund, K. M., Sakamoto, K. M., da Silva, A. M., Strawbridge, K. B., Strong, K., Taylor, J., Trigwell, R., Tereszchuk, K. A., Walker, K. A., Weaver, D., Whaley, C., and Young, J. C.: Quantifying the impact of BOReal forest fires on Tropospheric oxidants over the Atlantic using Aircraft and Satellites (BORTAS) experiment: design, execution and science overview, Atmos. Chem. Phys., 13, 6239–6261, doi:10.5194/acp-13-6239-2013, 2013. 22550

Paugam, R., Wooster, M., Papadakis, G., and Schultz, M.: Estimation of the injection height of biomass burning emission, in: Proceeding in the ESA-iLEAPS-EGU joint conference, Frascati, Italy, 3-5 November 2010, European Space Agency, 2010. 22565

ACPD
14, 22547–22585, 2014

Penner, J. E., Haselman, L. C., and Edwards, L. L.: Smoke-plume distributions above large-scale fires: implications for simulations of nuclear winter, Appl. Met., 25, 1434–1444, 1986. 22554

Pergaud, J., Masson, V., Malardel, S., and Couvreux, F.: A parameterization of dry thermals and shallow cumuli for mesoscale numerical weather prediction, Bound.-Lay. Meteorol., 132, 132–106, 2009. 22565

Pfister, G., Hess, P. G., Emmons, L. K., Lamarque, J.-F., Wiedinmyer, C., Edwards, D. P., Pétron, G., Gille, J. C., and Sachse, G. W.: Quantifying CO emissions from the 2004 Alaskan wildfires using MOPITT CO data, Geophys. Res. Lett., 32, L11809, doi:10.1029/2005GL022995, 2005. 22561

Pfister, G. G., Avise, J., Wiedinmyer, C., Edwards, D. P., Emmons, L. K., Diskin, G. D., Podolske, J., and Wisthaler, A.: CO source contribution analysis for California during ARCTAS-CARB, Atmos. Chem. Phys., 11, 7515–7532, doi:10.5194/acp-11-7515-2011, 2011. 22550

Potter, B. E.: The role of released moisture in the atmospheric dynamics associated with wildland fires, Int. J. Wildland Fire, 14, 77–84, 2005. 22554

Rienecker, M. M., Suarez, M., Todling, R., Bacmeister, J., Takacs, L., Liu, H.-C., Gu, W., Sienkiewicz, M., Koster, R., Gelaroa, R., Stajner, I., and Nielsen, J.: The GEOS-5 Data Assimilation System – Documentation of Versions 5.0.1, 5.1.0, and 5.2.0., 27, Technical Report Series on Global Modeling and Data Assimilation, NASA, Greenbelt, Maryland, 2008. 22553, 22555

Roberts, G., Wooster, M. J., and Lagoudakis, E.: Annual and diurnal african biomass burning temporal dynamics, Biogeosciences, 6, 849–866, doi:10.5194/bg-6-849-2009, 2009. 22556

Ross, A. N., Wooster, M. J., Boesch, H., and Parker, R.: First satellite measurements of carbon dioxide and methane emission ratios in wildfire plumes, Geophys. Res. Lett., 40, 4098–4102, doi:10.1002/grl.50733, 2013. 22549

Sessions, W. R., Fuelberg, H. E., Kahn, R. A., and Winker, D. M.: An investigation of methods for injecting emissions from boreal wildfires using WRF-Chem during ARCTAS, Atmos. Chem. Phys., 11, 5719–5744, doi:10.5194/acp-11-5719-2011, 2011. 22550

Shephard, M. W. and Edward, J. K.: Effect of band-to-band coregistration on fire property retrievals, Trans. Geos. Rem. Sens., 11, 2648–2661, doi:10.1109/TGRS.2003.814912, 2003. 22551

ACPD
14, 22547–22585, 2014

Streets, D. G., Zhang, Q., Wang, L., He, K., Hao, J., Wu, Y., Tang, Y., and Carmichael, G. R.: Revisiting China's CO emissions after the Transport and Chemical Evolution over the Pacific (TRACE-P) mission: Synthesis of inventories, atmospheric modeling, and observations, J. Geophys. Res., 111, D14306, doi:10.1029/2006JD007118, 2006. 22555

Luderer, G., Trentmann, J., and Andreae, M. O.: A new look at the role of fire-released moisture on the dynamics of atmospheric pyro-convection, Int. J. Wildland Fire, 18, 554–562, 2009. 22554

Trentmann, J., Luderer, G., Winterrath, T., Fromm, M. D., Servranckx, R., Textor, C., Herzog, M., Graf, H.-F., and Andreae, M. O.: Modeling of biomass smoke injection into the lower stratosphere by a large forest fire (Part I): reference simulation, Atmos. Chem. Phys., 6, 5247–5260, doi:10.5194/acp-6-5247-2006, 2006. 22554

Val Martin, M., Logan, J. A., Kahn, R. A., Leung, F.-Y., Nelson, D. L., and Diner, D. J.: Smoke injection heights from fires in North America: analysis of 5 years of satellite observations, Atmos. Chem. Phys., 10, 1491–1510, doi:10.5194/acp-10-1491-2010, 2010. 22560

Val Martin, M., Kahn, R. A., Logan, J. A., Paugam, R., Wooster, M., and Ichoku, C.: Space-based observational constraints for 1-D fire smoke plume-rise models, J. Geophys. Res., 117, D22204, doi:10.1029/2012JD018370, 2012. 22550, 22551, 22559

van der Werf, G. R., Randerson, J. T., Giglio, L., Collatz, G. J., Kasibhatla, P. S., and Arellano Jr., A. F.: Interannual variability in global biomass burning emissions from 1997 to 2004, Atmos. Chem. Phys., 6, 3423–3441, doi:10.5194/acp-6-3423-2006, 2006. 22549

van der Werf, G. R., Randerson, J. T., Giglio, L., Collatz, G. J., Mu, M., Kasibhatla, P. S., Morton, D. C., DeFries, R. S., Jin, Y., and van Leeuwen, T. T.: Global fire emissions and the contribution of deforestation, savanna, forest, agricultural, and peat fires (1997–2009), Atmos. Chem. Phys., 10, 11707–11735, doi:10.5194/acp-10-11707-2010, 2010. 22555

Wooster, M. J. and Zhang, Y. H.: Boreal forest fires burn less intensely in Russia than in North America, Geophys. Res. Lett., 31, L20505, doi:10.1029/2004GL020805, 2004. 22559

Wooster, M. J., Zhukov, B., and Oertel, D.: Fire radiative energy for quantitative study of biomass burning: derivation from the BIRD experi- mental satellite and comparison to MODIS fire products, Remote Sens. Environ., 86, 83–107, 2003. 22551, 22552

Wooster, M. J., Roberts, G., and Perry, G. L. W.: Retrieval of biomass combustion rates and totals from fire radiative power observations: FRP derivation and calibration relationships between biomass consumption and fire radiative energy release, J. Geophys. Res., 110, D24311, doi:10.1029/2005JD006318, 2005. 22550, 22551, 22552, 22554

ACPD
14, 22547–22585, 2014

Yevich, R. and Logan, J. A.: An assessment of biofuel use and burning of agricultural waste in the developing world, Global Biogeochem. Cy., 17, doi:10.1092/2002GB001952, 2003. 22555

Zhang, L., Li, Q. B., Jin, J., Liu, H., Livesey, N., Jiang, J. H., Mao, Y., Chen, D., Luo, M., and Chen, Y.: Impacts of 2006 Indonesian fires and dynamics on tropical upper tropospheric carbon monoxide and ozone, Atmos. Chem. Phys., 11, 10929–10946, doi:10.5194/acp-11-10929-2011, 2011. 22550

Zhukov, B., Lorenz, E., Oertel, D., Wooster, M., and Roberts, G.: Spaceborne detection and characterization of fires during the bi-spectral infrared detection (BIRD) experimental small satellite mission, Remote Sens. Environ., 100, 29–51, 2005. 22551

ACPD
14, 22547–22585, 2014

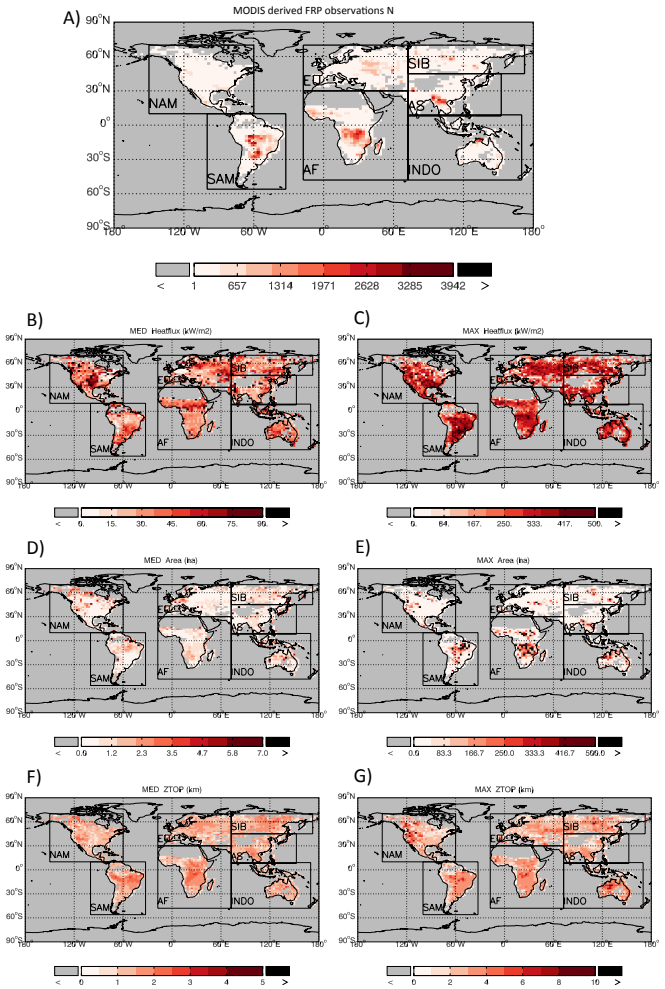

ACPD
14, 22547–22585, 2014

Pyroconvection using fire energy

S. Gonzi et al.

Figure 1. (A) Spatial distribution of the number of MODIS observations that fall into 2.0° × 2.5° GEOS-Chem grid boxes during 2006, and the median (MED) and maximum values (MAX) for **(B)** and **(C)** radiant heatflux (kW m^{-2}), **(D)** and **(E)** burnt area (hectares), **(F)** and **(G)** the resulting injection height ztop (km). The study regions include North America (NAM), South America (SAM), Europe (EU), Africa (AF), Siberia (SIB), Asia (AS), and Indonesia (INDO).

ACPD
14, 22547–22585, 2014

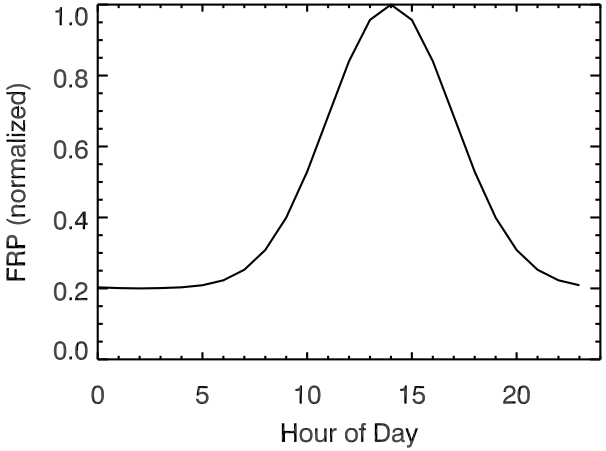

Figure 2. Daily normalized FRP diurnal cycle used in this study.

ACPD
14, 22547–22585, 2014

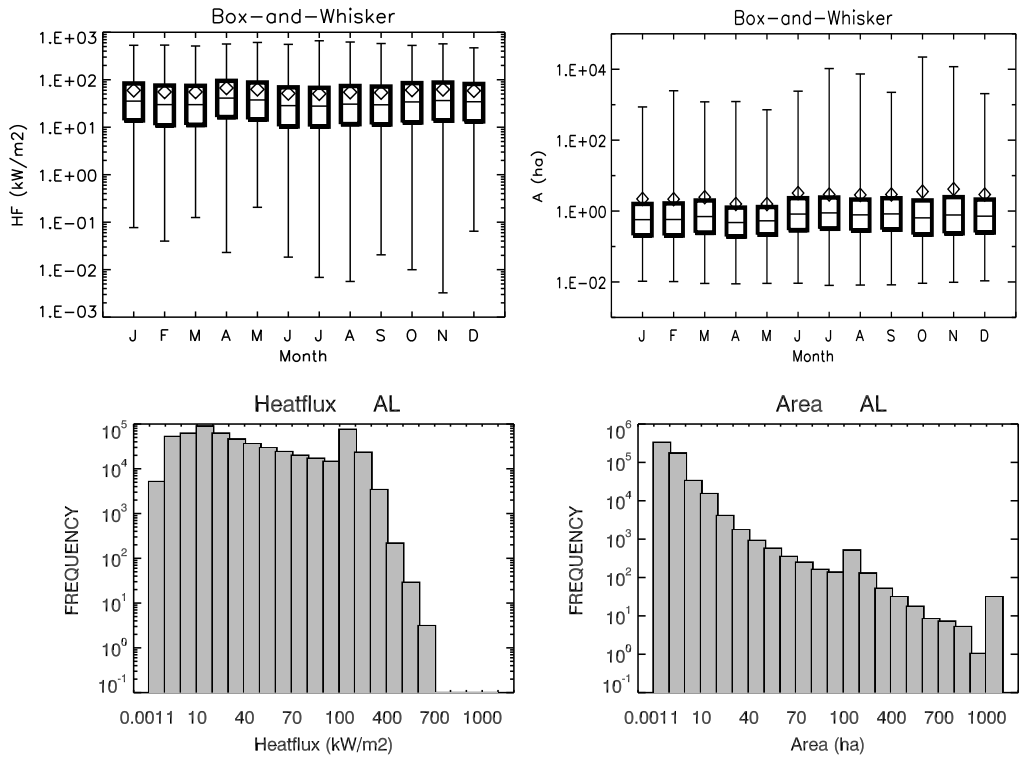

Figure 3. Box and whiskers (top row) and frequency distributions (bottom row) of convective heat flux HF (kW m^{-2}) and actual burnt area *A* (hectare) for the year 2006. For the box and whiskers plot the mean is denoted by the diamond and the median by a horizontal line within the box. The frequency distribution uses a logarithmic scale for heatflux and burnt area. The number of observation reported is approximately 562 000.

ACPD
14, 22547–22585, 2014

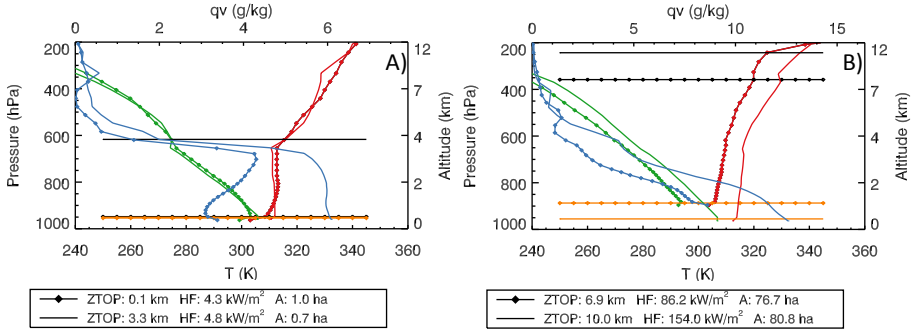

Figure 4. Sensitivity of injection height to varying atmospheric profiles of temperature (K) and specific humidity ($g\,Kg^{-1}$). The black and orange solid horizontal lines denote the injection height ZTOP (km) and local boundary layer heights, respectively. Red, green, and blue vertical profiles denote potential temperature, temperature, and specific humidity q_v ($g\,kg^{-1}$), respectively. The diamond marked lines denote the low injection height case. Convective heat flux (HF, $kW\,m^{-2}$), active fire size (A, ha) and corresponding injection height (ZTOP, km) are shown in panel-specific legends. Not all profiles start at 1000 hPa due to the local terrain. Panel **(A)** includes profiles over Africa ($+17.5^{\circ}/+10^{\circ}$) and over the Amazon basin ($-55^{\circ}/-14^{\circ}$) with ZTOP values of 0.1 km and 3.3 km, respectively. Panel **(B)** includes profiles over Canada ($-122^{\circ}/+56^{\circ}$) and over Australia ($+130^{\circ}/-20^{\circ}$) with ZTOP values of 3.3 km and 10.0 km, respectively.

ACPD
14, 22547–22585, 2014

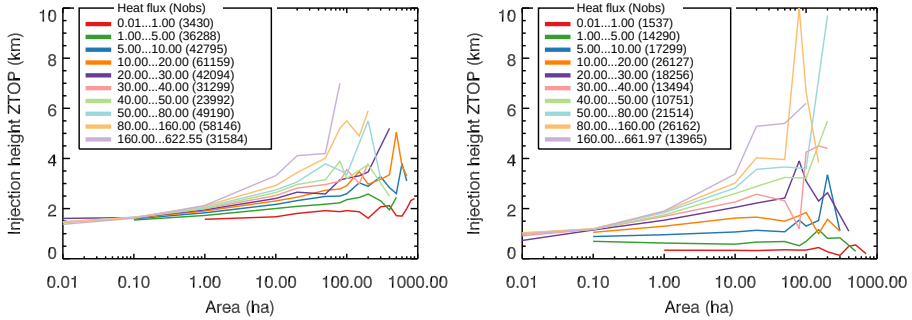

Figure 5. Injection heights as a function of MODIS derived active fire area (ha) and convective heat flux (kW m^{-2}) during 2006. The number of observations (N_{obs}) per bin of heat flux is given in parentheses. Left panel shows instances where there is a stable atmosphere in the first few levels determined by a positive vertical gradient in potential temperature and the right panel shows instances with an unstable atmosphere.

ACPD
14, 22547–22585, 2014




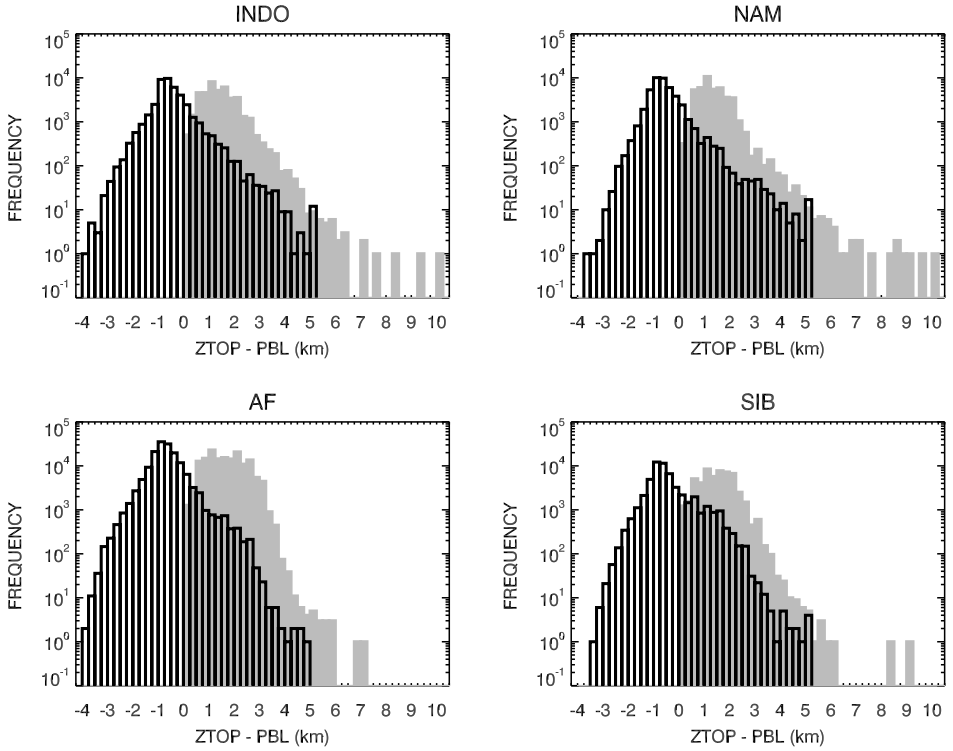

Figure 6. Distribution of injection height (ZTOP) minus the local boundary layer (PBL) + 250 m for four example burning regions around the globe: INDO (Indonesia), NAM (North America), AF (Africa), and SIB (Siberia). The grey area represents the distribution of injection heights. The ordinate is in log space.

ACPD
14, 22547–22585, 2014

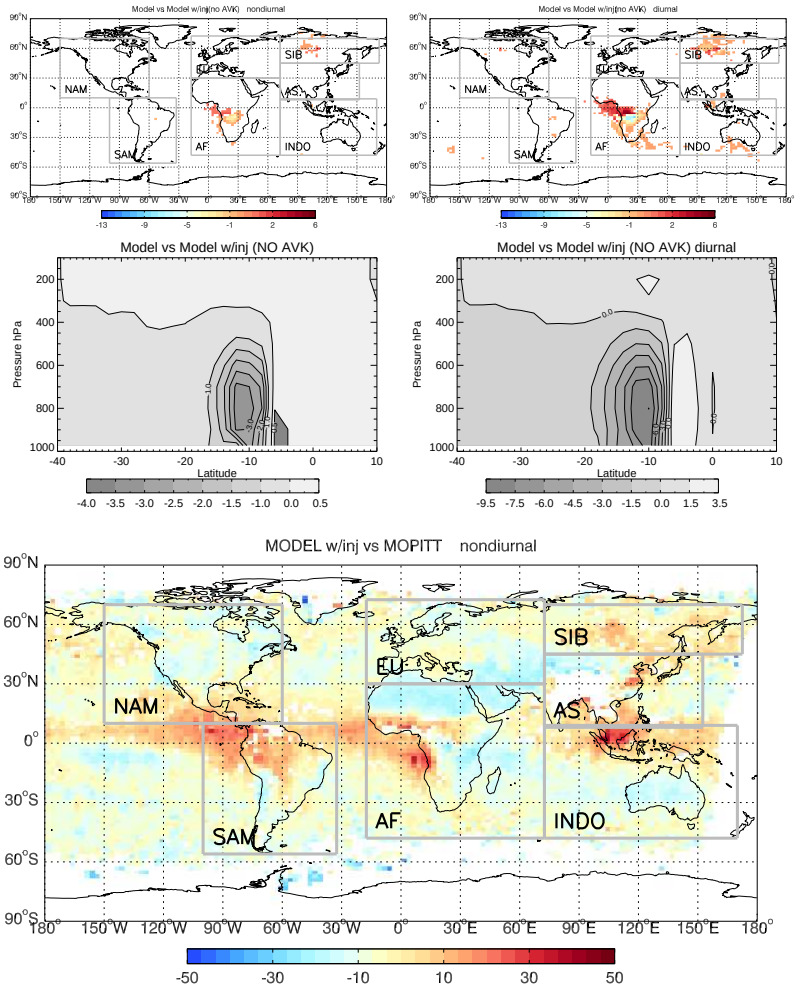

ACPD
14, 22547–22585, 2014

Pyroconvection using fire energy

S. Gonzi et al.

Figure 7. Top panel: CO total column bias (%) between model and model with injection height in GEOS-Chem space for the month of July 2006. Middle panel: CO concentration bias (%) along latitude vs altitude at ≈ 17° longitude. Bottom panel: CO total column bias (%) between model with injection height and MOPITT. Title indicates non diurnal (left) or diurnal (right) FRP cycle. White areas indicate a bias of ≈ 0 %.

ACPD
14, 22547–22585, 2014

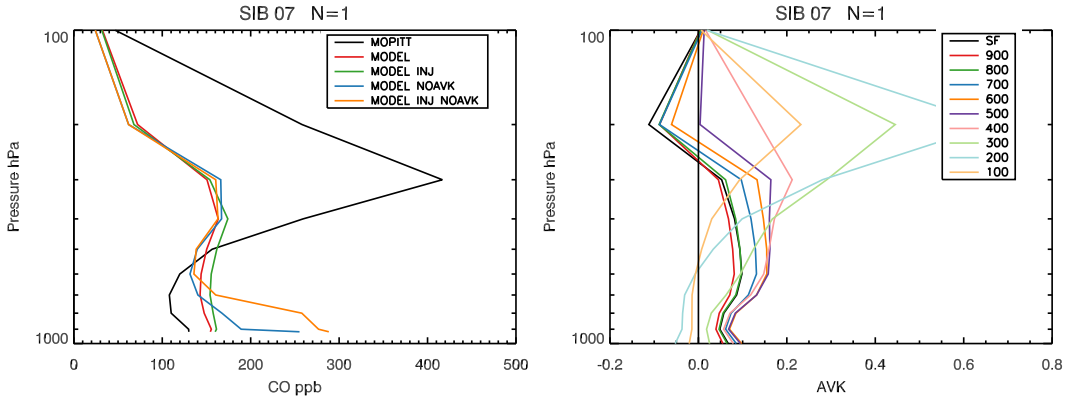

Figure 8. Observed CO profile from MOPITT in July 2006 over Siberia and comparison to model profiles (w/o injection height). NOAVK denotes the profiles in GEOS-Chem space. The title denotes the region and month. The model profiles shown here are for the diurnal FRP cycle. The right plot shows the corresponding MOPITT averaging kernels (AVK) from the surface (SF) to 100 hPa.

ACPD
14, 22547–22585, 2014